Averaged Anchoring of Decoupled Templates in a Tail-Energized Monoped

Avik De and Daniel E. Koditschek

Abstract We refine and advance a notion of parallel composition to achieve for the first time a stability proof and empirical demonstration of a steady-state gait on a highly coupled 3DOF legged platform controlled by two simple (decoupled) feedback laws that provably stabilize in isolation two simple 1DOF mechanical subsystems. Specifically, we stabilize a limit cycle on a tailed monoped to excite sustained sagittal plane translational hopping energized by tail-pumping during stance. The constituent subsystems for which the controllers are nominally designed are: (i) a purely vertical bouncing mass (controlled by injecting energy into its springy shaft); and (ii) a purely tangential rimless wheel (controlled by adjusting the inter-spoke stepping angle). We introduce the use of averaging methods in legged locomotion to prove that this "parallel composition" of independent 1DOF controllers achieves an asymptotically stable closed-loop hybrid limit cycle for a dynamical system that approximates the 3DOF stance mechanics of our physical tailed monoped. We present experimental data demonstrating stability and close agreement between the motion of the physical hopping machine and numerical simulations of the (mathematically tractable) approximating model.

1 Introduction

Dimension reduction enjoys a long analytical tradition in dynamical systems theory generally [1] and locomotion particularly [2], but the synthesis of complex, high dimensional dynamical behavior from simple low dimensional components is far less considered. Notwithstanding some early examples of anchored templates [3] in physical [4, 5] and numerical [6, 7] studies, the only presently available systematic account of how to embed low dimensional target dynamics in higher dimensional mechanical bodies entails inverse dynamics along the quotient space down to the

attracting submanifold [8, 9]. Yet well before any of this work, Raibert had already shown empirically how to synthesize stable one-, two-, and four-legged spatial running behavior by parallel composition of simple, decoupled, one degree of freedom vertical, horizontal, and rotational feedback laws [10].

Motivation and contributions   This paper builds on and significantly advances the ideas of [11, 12] to achieve what we believe to be the first formal account of such anchor synthesis via template composition. We examine an approximate model of a tailed monoped that exhibits stable sagittal plane translational hopping motion energized by tail pumping during stance. The tail controller excites its actuator by applying a new purely vertical hopping regulator [13] to the the robot's shank oscillation phase. The stepping controller adjusts the next leg touchdown angle by applying a modified active rimless wheel speed regulator [14] to the angular momentum of the robot's mass center relative to the pinned toe. We show that both the vertical and fore-aft regulators, acting alone on their respective one degree of freedom template plants in isolation, succeed in stabilizing hopping height and horizontal speed. We then show that this parallel composition of template controllers stabilizes the hopping translational gait of the highly coupled approximate model.[1]

This paper introduces as well (to the best of our knowledge for the first time) in the locomotion literature the dynamical systems methodology of averaging. Harnessing specific symmetries in motion and force played a major role in Raibert's compositional methods [10] and we express his intuition here by integrating them out (or in) along the stance phase. Such appeal to averaging symmetric dynamical influences gains its theoretical traction [1, 15] because our mechanical system executes periodic orbits in its locomotory steady state along which (loosely speaking) the energy levels of various compartments of the dynamics evolve at a much slower time-scale than does the phase. The right confluence of these circumstances has the fortunate effect of insuring not only that the averaged dynamics closely approximate the original but guaranteeing that their steady state (limit cycle stability) properties are identical. Recourse to averaging, in turn, motivates a new, relaxed version of the template-anchor relation [3]. We develop this new idea using our motivational example in Section 4, but we leave a formal definition to future work.

Organization and results   We first develop some mathematical tools for averaging a particular class (Def. 1) of hybrid systems in Section 2. Prop. 1 extends the classical averaging result [1] to our application domain. An application-focused reader may skip this section initially and refer back at its usage in Sections 3-4.

In Section 3, we present two classical 1DOF template systems as phase-averageable hybrid systems: the vertical hopper [13] and the rimless wheel [16] (modified to include some control affordance [14]). We present template controllers for these template systems (inspired by [10, 17]) that provably stabilize the 1DOF plants.

In Section 4, we show how to take the parallel composition of these two simple constituents and apply it to a 3DOF model of the tailed SLIP (an approximation to

---

[1] The chief advances beyond the initial composition study of [11] are that: (i) we achieve a stability proof of the steady state gait limit cycle for the 4DOF closed loop tailed biped (Fig. 1); and (ii) we are able to do so for a far less restricted range of tail-energizing energies (17).

a physical system that we have built). We use averaging theory to demonstrate that the desired steady state hopping behavior is indeed rendered asymptotically stable in this highly coupled 3DOF model.

In Section 5 we show simulation evidence for our theoretical claims, and data from a physical hopping machine showing (in spite of our approximations in the model of Section 4) qualitative behavior quite similar to the simulation results.

The contributions of this paper can be summarized as (a) introduction of a new notion of "average anchoring," and an extension of classical averaging theory (Prop. 1) to a relevant class of hybrid systems, (b) "unpacking" the classic SLIP template [18] as a "cross-product" (in our relaxed sense of anchoring) of a vertical heartbeat [13] and a rimless wheel [16], and (c) a proof of stability of compositional control using decoupled controllers in a coupled 3DOF tailed SLIP model system.

A note on notation The symbol $a_\star$ refers to an "energy" coordinate for subsystem $\star$ (not necessarily mechanical energy), which changes slowly relative to the phase of the system (Defn. 1). The bold subscript is also used for other symbols pertaining to a specific subsystem; e.g. $k_\mathbf{v}$ is the gain chosen for the **v**ertical subsystem. We have collected references to important equations and symbols in Table 1.

2 Hybrid Averaging

For our analysis in this paper will focus on hybrid systems with a single domain. We specialize the general definition in [19], of a hybrid system with 1 domain, to add properties conducive to averaging (Prop. 1).

Definition 1. Given $\varepsilon > 0$ (a "separation of time scales" parameter quantifying slow energy-phase dynamics), an *averageable hybrid system* is a tuple $(\mathcal{A}, f, \mathcal{R})$ with

  i) a topological disk $\mathcal{A} \approx \mathbb{R}^d$ as the "energy" domain,
  ii) a C^2 non-autonomous ("phase-varying") vector field $f : \mathcal{A} \times [0, T_s] \times \mathbb{R}_+ \to T\mathcal{A}$, where $T_s > 0$, such that the system dynamics are

$$\dot{x} = \varepsilon f(x, t, \varepsilon), \text{ and} \tag{1}$$

  iii) an energy reset map, $\mathcal{R} : \mathcal{A} \to \mathcal{A}$ that is ε-close to the identity in the sense that there is some array-valued smooth map, $S(x)$ such that the equilibrium of f is also a fixed point of R, and the Jacobian of $\mathcal{R}$ is $D\mathcal{R} = I + \varepsilon S$, and $S(x) + T_s Df(x)$ is full rank at each x.

Remark Though the definition above is sufficient for this paper, we observe that the triple $(\mathcal{A}, f, \mathcal{R})$ is a mere specialization of a hybrid system as defined in [19, Def. 1]. To see how, think of decoupled "phase" dynamics $\dot{\psi} = \omega$ being appended to the state, yielding a standard hybrid system $H = (D, F, G, R)$, where $D := \mathcal{A} \times [0, T_s]$, $F := \begin{bmatrix} \omega f \end{bmatrix}$, $G := \mathcal{A} \times \{T_s\}$, $R := \begin{bmatrix} \mathcal{R} \\ 0 \end{bmatrix}$ with a single hybrid mode. The last condition above is difficult to check, and we leave a more complete generalization of this result to future work.

The "averaging" technique [1] can be extended to a method of approximating (with error bounds) solutions of the T_s-periodic system (1) with an *averaged hybrid system* by replacing f in (1) with

$$\frac{dx}{dt} = \frac{\varepsilon}{T_s} \int_0^{T_s} f(x,t,0)\,dt =: \varepsilon\overline{f}(x), \tag{2}$$

with the same decoupled phase, guard set and reset map.

Additionally, the Poincaré return maps for (1) and (2) can both be defined as usual, using $\mathcal{A} \times \{T_s\}$ as the section.

Proposition 1 (Hybrid averaging). *Let $(\mathcal{A}, f, \mathcal{R})$ be a averageable hybrid system. If p_0 is a hyperbolic fixed point of an equilibrium of (2), then there exists $\varepsilon_0 > 0$ such that for all $0 < \varepsilon \le \varepsilon_0$, (1) possesses a unique hyperbolic periodic orbit $r(p_0) + \mathcal{O}(\varepsilon)$, of the same stability type as p_0.*

Proof (adapted from [1]). Our system satisfies all conditions required for the proof of Thm. 4.1.1(i) in [1] on the set $t \in (0, T_s]$. We conclude that if at $\psi = 0^+$ (just after the reset), $|x_0 - y_0| = \mathcal{O}(\varepsilon)$, then $|x(t) - y(t)| = \mathcal{O}(\varepsilon)$ on a time scale $t \sim 1/\varepsilon$. Construct the change of coordinates $x = y + \varepsilon w(y, t, \varepsilon)$, as in [1], so that (1) becomes

$$\frac{dy}{dt} = \varepsilon\overline{f}(y) + \varepsilon^2 f_1(y, t, \varepsilon), \tag{3}$$

where f_1 is a lumped $\mathcal{O}(\varepsilon^2)$ "remainder term."

With the cross-section $\Sigma := \{(y, t) : t = T_s\}$, and $U \subset \Sigma$, an open set, the Poincaré maps $P_0 : U \to \Sigma$ and $P_\varepsilon : U \to \Sigma$ can be defined as usual (reset composed by a flow for time Ts) for the systems (2) and (3), respectively. P_ε is ε^2-close to P_0, since (a) r is the same for both, and (b) the "time to impact" is fixed and independent of ε (decoupled phase dynamics).

Since p_0 is a hyperbolic fixed point of P_0, it is also a hyperbolic fixed point of $\mathrm{D}P_0(p_0) = e^{\varepsilon T_s \mathrm{D}f(\mathcal{R}(p_0))}\mathrm{D}\mathcal{R}(p_0)$ ($\mathrm{D}\mathcal{R}$ is full rank for diffeomorphism $\mathcal{R}$). Therefore, substituting $\mathrm{D}r = I + \varepsilon S$, the matrix

$$\lim_{\varepsilon \to 0} \frac{1}{\varepsilon}(\mathrm{D}P_0(p_0) - I) = \lim_{\varepsilon \to 0}\frac{1}{\varepsilon}(I + \varepsilon T_s \mathrm{D}f|_{\mathcal{R}(p_0)})\mathrm{D}\mathcal{R}(p_0) - I$$
$$= S + T_s \mathrm{D}f|_{\mathcal{R}(p_0)} \tag{4}$$

is invertible (from the resonance-free condition of Prop. 1). Since P_ε is ε-close to P_0, $\lim_{\varepsilon \to 0}\frac{1}{\varepsilon}(\mathrm{D}P_\varepsilon(p_0) - I)$ is the same as the RHS of (4). Hence, using the implicit function theorem we see that the rank of $\frac{1}{\varepsilon}(\mathrm{D}P_\varepsilon(p_0) - I)$ form a smooth curve $(p_\varepsilon, \varepsilon)$. Now p_ε is a fixed point of P_ε, and the local Taylor expansion is $p_\varepsilon = p_0 + \mathcal{O}(\varepsilon)$. The eigenvalues of $\mathrm{D}P_\varepsilon(p_\varepsilon)$ are ε^2-close to those of $\mathrm{D}P_0(p_0)$, since $\mathcal{R}$ is a diffeomorphism, and

$$\mathrm{D}P_\varepsilon = [\exp(\varepsilon T_s \mathrm{D}f|_{\mathcal{R}(p_0)}) + \mathcal{O}(\varepsilon^2)] \cdot \mathrm{D}\mathcal{R}(p_0).$$
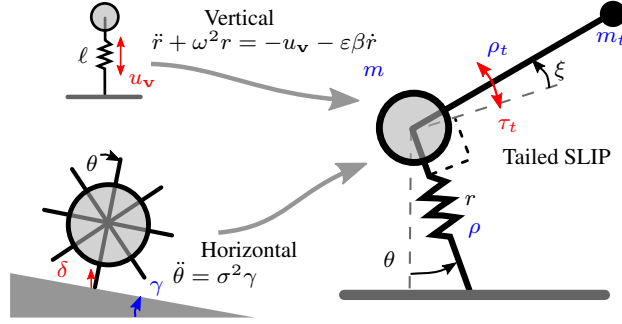
Fig. 1 The vertical hopper [13] and rimless wheel [16] template plants (**left**), and their corresponding equations of motion, and (**right**) the tailed SLIP model, labeled with configuration variables (black), actuators (red), and model parameters (blue).

Table 1 References to decoupled controllers and important ODE's and vector fields.

	Vertical hopper	Rimless wheel	Anchor
Controller	$u_{\mathbf{v}}$ (8)	$u_{\mathbf{h}}(a_{\mathbf{h}})$ (13)	$\approx u_{\mathbf{v}}(t) \times u_{\mathbf{h}}(a_{\mathbf{h}})$ (16), (23)
Dynamics	$\ddot{r}$ (5), $f_{\mathbf{v}}$ (9)	$\ddot{\theta}$, $f_{\mathbf{h}}$ (11)	$\ddot{\mathbf{q}}$ (15)
Averaged dynamics	$\overline{f}_{\mathbf{v}}$ (10)	$\overline{f}_{\mathbf{h}} = f_{\mathbf{h}}$ (11)	$\overline{f} = \overline{f}_{\mathbf{v}} \times \overline{f}_{\mathbf{h}}$ (19), (22)

So, (3) has a periodic orbit ε-close to $\mathcal{R}(p_0)$, and by the coordinate change (3), (1) has a similar orbit. The stability properties of the periodic orbits of (1) and (2) are identical since $\mathrm{D}P_\varepsilon(p_\varepsilon)$ is ε^2-close to $\mathrm{D}P_0(p_0)$. ∎

3 Templates as Constituents of Planar Hopping

Based on the motivation in Section 1, we attempt to develop a planar hopping behavior as a composition of (a) a vertical hopper, as empirically demonstrated by [10] and studied in [13, 11], and (b) a rimless wheel [16] with liftoff impulses [14]. As Fig. 1 notionally shows, these templates are "anchored" (Section 4) in the Tailed SLIP model our physical platform (Section 5) closely resembles.

3.1 Controlled 1DOF Vertical Hopper

Our template plant for vertical hopping is a point mass connected to a vertically-constrained series-elastic damped leg (Fig. 1, top left). As shown in [11], this 1DOF system can be stabilized to arbitrary hopping heights by recourse to an appropriately designed phase-locked, oscillatory pattern of energetic excitation entering through

the shank (note the contrast to the hybrid energization strategy of [10, 13]). We impose the following additional assumption and follow [11]:

Assumption 1 (Weakly nonlinear oscillator). *The vertical hopper is an LTI spring-mass-damper system actuated by a possibly nonlinear $\mathcal{O}(\varepsilon)$ force, where $\varepsilon \ll \omega$.*

Stance dynamics Define the normalized leg length $r := \widetilde{r} - \rho + mg/\omega^2$, where $\widetilde{r}$ is the physical length of the spring with rest length ρ. As in [11], the dynamics of a linear oscillator with small (assumption 1) damping are given by

$$\ddot{r} + \omega^2 r = -u_{\mathbf{v}} - \varepsilon\beta\dot{r} \implies \dot{x} = -\omega \begin{bmatrix} 0 & -1 \\ 1 & 0 \end{bmatrix} x + \begin{bmatrix} 0 \\ -u_{\mathbf{v}}/\omega - \varepsilon\beta x_2 \end{bmatrix}, \quad (5)$$

where $x := \begin{bmatrix} r \\ \dot{r}/\omega \end{bmatrix}$. Define the *vertical energy* $a_{\mathbf{v}} := \|x\|$, and note that by assumption 1, for $u_{\mathbf{v}} = \mathcal{O}(\varepsilon)$, the corresponding phase coordinate is trivial; if $\tan \angle x := -x_1/x_2$ (such that "stance" is from $\angle x = 0$ to π), then

$$\frac{d}{dt}\angle x = -\omega - \frac{\varepsilon\beta x_1 x_2}{a_{\mathbf{v}}^2} - \frac{u_{\mathbf{v}} x_1}{a_{\mathbf{v}}^2 \omega} = -\omega + \mathcal{O}(\varepsilon). \quad (6)$$

Thus the phase evolution is in the form of a perturbation problem [15, (10.1)]. The nominal system, $\frac{d}{dt}\angle x = -\omega$ has a trivial solution $(\angle x)_{\text{nom}} = -\omega t$. Using [15, Thm. 10.1], we conclude that for small ε, the perturbed system has a unique solution of the form $\angle x = -\omega t + \mathcal{O}(\varepsilon)$. Note that no "constant of integration" appears since at $t = 0$ (touchdown), $r(0) = 0, \dot{r}(0) < 0$, and so $\angle x(0) = 0$. Consequently,

$$x_2 = a_{\mathbf{v}} \cos \angle x = a_{\mathbf{v}} \cos(-\omega t + \mathcal{O}(\varepsilon))$$
$$= a_{\mathbf{v}}\big(\cos \omega t \cos(\mathcal{O}(\varepsilon)) + \sin \omega t \sin(\mathcal{O}(\varepsilon))\big) = a_{\mathbf{v}}(\cos \omega t + \mathcal{O}(\varepsilon)), \quad (7)$$

since $\cos(\mathcal{O}(\varepsilon)) = 1 - \mathcal{O}(\varepsilon^2)$ and $\sin(\mathcal{O}(\varepsilon)) = \mathcal{O}(\varepsilon)$. Following [11], set

$$u_{\mathbf{v}} := -\varepsilon k_{\mathbf{v}} \omega \cos \omega t, \quad (8)$$

and observe that

$$\dot{a}_{\mathbf{v}} = \varepsilon f_{\mathbf{v}}(a_{\mathbf{v}}, t, \varepsilon) := \frac{\varepsilon x_2}{a_{\mathbf{v}}}(k_{\mathbf{v}} \cos \omega t - \beta x_2) \quad (9)$$

$$\approx \varepsilon \overline{f}_{\mathbf{v}}(a_{\mathbf{v}}) := \frac{\varepsilon}{\pi/\omega} \int_0^{\pi/\omega} f_{\mathbf{v}}(a_{\mathbf{v}}, t, 0)\, dt = \frac{\varepsilon}{2}(k_{\mathbf{v}} - \beta a_{\mathbf{v}}), \quad (10)$$

where the bottom row corresponds to a usage of Prop. 1 on the limit cycle, and we used (7) to eliminate $\mathcal{O}(\varepsilon^2)$ terms.

Hybrid guard and reset For this system and our periodic forcing (8), we observe that the dynamics (9) are π/ω-periodic. Roughly following [13], we collapse the "flight map" to a reflection of the vertical velocity, or $\mathcal{R}_{\mathbf{v}}(a_{\mathbf{v}}) = a_{\mathbf{v}}$, and the guard set is $G_{\mathbf{v}} = \{x_1 = 0\}$ (lift-off occurs approximately at adjusted rest length).

Return map stability From the simple from (10), it is easy to see that the averaged hybrid system has a stable limit cycle at $a_\mathbf{v} = k_\mathbf{v}/\beta$, and hence by Prop. 1, we can conclude that the vertical hopper plant (5) has a stable limit cycle.

3.2 Controlled Forward Speed: 1DOF Active Rimless Wheel

Our conceptual physical template for an isolated fore-aft system stabilized by "stepping" is inspired by the rimless wheel due to [16] (parameters defined in Fig. 1), but now fitted out with a controllable liftoff impulse, δ (inspired by [14]).

Assumption 2 (Gravity approximation). *As in [20], we assume that the effect of gravity is invariant to leg angle.*

The conservative approximation is useful in our search for *sufficient* conditions for an analytical stability proof (Prop. 3), but we empirically observe stability with large leg angles (Section 5), indicating that it is not necessary.

Stance dynamics The implication of assumption 2 on the rimless wheel (physically manifested when the interspoke angle is small compared to the slope angle) is that angular acceleration is roughly constant through stance. Using notation from [16], and angular momentum about the toe $a_\mathbf{h} := \ell^2 \dot{\theta}$ as the *horizontal energy*,

$$\ddot{\theta} = \sigma^2 \gamma \implies \dot{a}_\mathbf{h} = \varepsilon f_\mathbf{h} := \sigma^2 \gamma/\ell^2, \tag{11}$$

where σ is a dimensionless frequency and ℓ is the spoke length (Fig. 1) [16]. We observe that the right hand side is a constant, hence bounded.

Reset From [16, (5)], the rimless wheel has a restitution coefficient $\eta := 1 - \sigma^2(1 - \cos 2\alpha_0)$. The controlled reset map (with our modification to [16, (3)]) is

$$a_\mathbf{h}^+ = a_\mathbf{h}\eta + \delta = a_\mathbf{h} + u_\mathbf{h}, \tag{12}$$

where in the last equality, we parameterize the liftoff impulse as $\delta = (1-\eta)a_\mathbf{h} + u_\mathbf{h}$ for notational convenience. Using the discrete proportional controller (suggested by the "stepping" controller [10]) with $k_\mathbf{h} \ll 1$,

$$u_\mathbf{h}(a_\mathbf{h}) = k_\mathbf{h}(a_\mathbf{h}^* - a_\mathbf{h}), \tag{13}$$

the controlled reset map becomes $\mathcal{R}_\mathbf{h}(a_\mathbf{h}) = a_\mathbf{h} + k_\mathbf{h}(a_\mathbf{h}^* - a_\mathbf{h})$. The guard set is $\{\theta = -\alpha_0\}$.

Return map stability The integrable stance dynamics (11) together with the reset map above give us the closed-form return map

$$P_\mathbf{h}(a_\mathbf{h}) := a_\mathbf{h} + k_\mathbf{h}(a_\mathbf{h}^* - a_\mathbf{h}) + \nu_0, \tag{14}$$

Fig. 2 A cartoon depicting the classical notion of anchoring [3] **(top)** and the new notion introduced in this paper based on averaging **(bottom)** as conceptual mechanisms of dimension reduction (Section 1), where the blue line represents a *template* flow, and the red lines depict flows on the anchoring body.
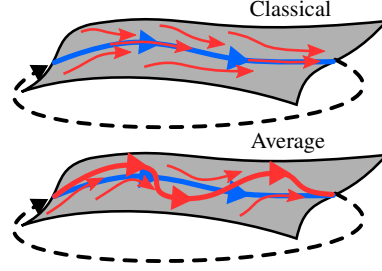
where $\nu_0 := \int_0^{T_s} \sigma^2 \gamma / \ell^2 \, dt$ is the leg sweep over a fixed stance duration T_s. The Jacobian is $\mathrm{D}P_{\mathbf{h}}(a_{\mathbf{h}}) = 1 - k_{\mathbf{h}}$, and so the system will stabilize at the fixed point $a_{\mathbf{h}} = a_{\mathbf{h}}^* + \nu_0 / k_{\mathbf{h}}$.

Remarks Both the continuous (11) and discrete (14) parts of the dynamics exhibit a θ-equivariance, and since an encoding of a planar hopping task [10, Chap. 2] is also θ-invariant, we work in the quotient space with coordinates given by the simple projection $(\theta, \dot{\theta}) \mapsto a_{\mathbf{h}}$, mapping the second order system (11) to an energy coordinate without a corresponding phase.

4 Average Anchoring in 3DOF Tail-Energized SLIP

The classical notion [3] of anchoring calls for the template dynamics (blue arrows in the top picture of Fig. 2) to be embedded in that of the anchoring body as an attracting invariant submanifold (red arrows in that same picture) of the left hand with conjugate restriction dynamics (depicted by the red lining up with blue arrows on the embedded submanifold). Averaging theory guarantees that the anchor must have a stable cycle (red arrows in the bottom picture of Fig. 2) that is close to an embedding of the template's (blue arrows, again, in the bottom picture), but the actual unaveraged (time-varying) anchor will in general have no related invariant manifolds nor dynamical conjugacy.

Our candidate "anchoring" body is a planar pogo stick with a light tail (Fig. 1), where the actuator τ_t is connected between the leg and the tail. In stance phase, the toe of the springy leg is pinned to the ground, and as a result, the robot is dynamically constrained to 3-DOF. Even though the body has two masses, the dynamics are somewhat simplified by the following assumption:

Assumption 3 (Light tail). *The tail mass is small, i.e. $m_t \ll m$ (such that the center of mass is configuration-independent), but the tail inertia, $i_t := m_t \rho_t^2$, is significant.*

Looking ahead to (15), this assumption allows us to use the tail as an inertial actuator on the leg spring through τ_t even though $m_t \ll m$, while avoiding Coriolis forces due to motion of the center of mass.

4.1 Average Invariance of Template Flows in Stance Dynamics

In this subsection, we examine the stance behavior of the coupled tailed monoped in steady-state operation (we examine stability in the next subsection). The present method of proof requires (what simulation and empirical results suggest to be) a conservative assumption of operation in a slow fore-aft speed regime:

Assumption 4 (Slow fore-aft speed)**.** *The leg angular velocity $\dot{\theta} = \mathcal{O}(\varepsilon)$, or equivalently, the leg sweep is $\mathcal{O}(\varepsilon)$ of π/ω.*

Additionally, we make a physically reasonable assumption about leg deflection:

Assumption 5. *The leg deflection relative to its rest length is $a_{\mathbf{v}}/\rho = \mathcal{O}(\varepsilon)$.*

Stance dynamics We use assumption 3 (specifically, taking a limit $m_t/m \to 0$ with finite i_t) in a Lagrangian formulation with variables as in Fig. 1, to get the following stance dynamics (3 of the 4 DOF's in [12, (39)]):

$$\ddot{r} = -\omega^2 r - \varepsilon\beta\dot{r} + \widetilde{r}\dot{\theta}^2 - \frac{\tau_t \cos\xi}{\rho_t m} + g(1 - \cos\theta),$$

$$\ddot{\theta} = -\frac{2\dot{r}\dot{\theta}}{\widetilde{r}} - \frac{\tau_t \sin\xi}{\rho_t m\widetilde{r}} - \frac{g}{\widetilde{r}}\sin\theta,$$

$$\ddot{\xi} = \tau_t/i_t, \tag{15}$$

where ξ is the leg-tail angle (between which joints τ_t acts directly), r is the normalized leg extension as in Section 3.1, and β is now the mass-specific damping coefficient. Our specific usage of assumption 3 in the equations of motion is that

- we assert that $m_b + m_t \approx m_b$, resulting in the dropping of Coriolis forces resulting from the configuration-dependent CoM,
- the tail can now be thought of as an inertial source of reaction forces on the $(\ddot{r}, \ddot{\theta})$ terms (which have familiar "SLIP-like" dynamics), as seen in the τ_t terms coupled through the physical tail angle, ξ).

We introduce as a stance controller for the coupled plant (15) a scaled version of the simple stance controller for the isolated vertical system (8),

$$\tau_t := m\rho_t u_{\mathbf{v}} = \varepsilon k_{\mathbf{v}}\omega m\rho_t \cos\omega t. \tag{16}$$

Decoupled tail excitation The tail dynamics, $\ddot{\xi}$, take the form of a simple double integrator (15). When driven by the template controller (Table 1), and reset to $\xi(0) = -\frac{\varepsilon k_{\mathbf{v}} m\rho_t}{\omega i_t}$ during flight, the tail trajectory is

$$\xi(t) = -\frac{\varepsilon k_{\mathbf{v}} m\rho_t}{\omega i_t}\cos\omega t =: -a_{\mathbf{t}}\cos\omega t, \tag{17}$$

where, for the purposes of design, we construe the amplitude of the tail oscillation as the energy contained in the tail compartment. Note that this represents a substantial

generalization and thus a significant advance beyond the strict assumptions in [11] regarding the analysis of a similar planar hopping model: in this paper we allow for finite (and possibly large) tail motions, which couple into the other DOFs (15).

Proposition 2. *The averaged tailed SLIP stance vector field—but not the unapproximated one, obtained from* (15)*—is conjugate to a cross product of the averaged template vector fields* (10)*,* (11)*.*

Proof. Because it is a decoupled double integrator, the feedforward influence of the tail subsystem (the output of the last row of (15), on the (r, θ) dynamics) can be represented as an independent time varying disturbance input, ξ, given in (17).

In the radial dynamics from (15), as in Section 3.1, let $x := \begin{bmatrix} r \\ \dot{r}/\omega \end{bmatrix}$. Reusing assumption 1, the phase of the vertical hopper is interchangeable with time, $\angle x = -\omega t$. Similar to (9), setting $a_{\mathbf{v}} := \|x\|$, and using (17),

$$\dot{a}_{\mathbf{v}} = \varepsilon f_{\mathbf{v}}(a_{\mathbf{v}}, t, \varepsilon) = \varepsilon \cos^2 \omega t \left(k_{\mathbf{v}} \cos\left(-a_{\mathbf{t}} \cos \omega t\right) - \beta a_{\mathbf{v}} \right) + \mathcal{O}(\varepsilon^2) \qquad (18)$$

$$\approx \varepsilon \overline{f}_{\mathbf{v}}(a_{\mathbf{v}}) = \frac{\varepsilon}{\pi/\omega} \int_{\mathbb{S}} f_{\mathbf{v}}(a_{\mathbf{v}}, t, 0) \, dt = \frac{\varepsilon}{2} (\widetilde{k}_{\mathbf{v}} - \beta a_{\mathbf{v}}), \qquad (19)$$

where the $\mathcal{O}(\varepsilon^2)$ term in (18) consists of the following terms from the first row of (15), and the vertical "phase lock error" (7):

$$\widetilde{r} \dot{\theta}^2 + g(1 - \cos \theta) - \varepsilon \beta a_{\mathbf{v}} \mathcal{O}(\varepsilon), \qquad (20)$$

and use assumption 4 to get $\dot{\theta}^2 = \mathcal{O}(\varepsilon^2)$ as well as $1 - \cos \theta \approx \theta^2/2 = \mathcal{O}(\varepsilon^2)$.

In (19), $\widetilde{k}_{\mathbf{v}} := k_{\mathbf{v}}(2J_1(a_{\mathbf{t}})/a_{\mathbf{t}} - J_2(a_{\mathbf{t}}))$, and J_i are Bessel functions of the first kind [21] that act as an "attenuation" of our vertical gain $k_{\mathbf{v}}$ (bear in mind that $a_{\mathbf{t}}$, introduced in (17) is a designed energizing magnitude term held constant for the duration of each stance), as the tail sweep gets larger (cf. Fig. 3).

In the leg-angle dynamics, define $a_{\mathbf{h}} := \widetilde{r}^2 \dot{\theta}$ as in the template (Section 3.2), and use assumption 2, and assumption 5 in the averaging step, to get:

$$\dot{a}_{\mathbf{h}} = \varepsilon f_{\mathbf{h}}(a_{\mathbf{h}}, t, \varepsilon) = -\varepsilon k_{\mathbf{v}} \omega \cdot m \rho_t \cos \omega t \left(\frac{\rho(1 - a_{\mathbf{v}}/\rho \sin \omega t) \sin \xi}{m \rho_t} \right) \qquad (21)$$

$$\approx \varepsilon \overline{f}_{\mathbf{h}}(a_{\mathbf{h}}) = -\varepsilon k_{\mathbf{v}} \omega \cdot \rho J_1(a_{\mathbf{t}}), \qquad (22)$$

where $J_1(a_{\mathbf{t}})$ amplifies (with the sign convention of Fig. 1, $a_{\mathbf{h}} < 0$ when the robot is making forward progress) the fore-aft acceleration as shown in Fig. 3.

Comparing (19) to (10), and (22) to (11), we see that the averaged body dynamics are conjugate to the template dynamics. Moreover, it is clear that (9) and (18) are not conjugate vector fields, and neither are (11) and (21). □

Remark Compared to classical anchoring [3], conjugacy of averaged fields is the analogue of the invariance of the embedded submanifold. However, note that there is no analogue of the "attraction" property yet (i.e. do asymmetric orbits attract to more symmetric ones?). We aim to study the "transient" behavior in future work.

Fig. 3 Gain scaling terms $\widetilde{k}_{\mathbf{v}}/k_{\mathbf{v}}$ (blue, (19)) and $J_1(a_{\mathbf{t}})$ (orange, (22)), as a function of the tail sweep. As $a_{\mathbf{t}} \to 0$, we recover the unscaled vertical template dynamics, but with larger tail sweep (the thin vertical line corresponds to empirically observed tail sweeps from Section 5), the equilibrium hopping height decreases, and the forward speed increases.
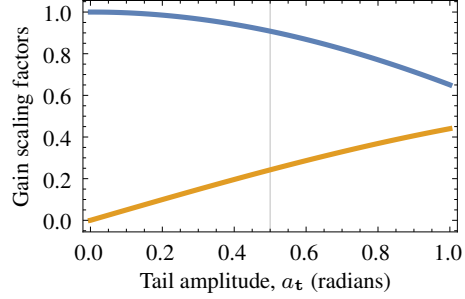
4.2 Stability Derived from Templates

The strong relation between the averaged and unaveraged systems guaranteed by Prop. 1 allows us to conclude existence of a periodic orbit as well as its hyperbolic stability type from that of the averaged system, which we calculate below.

Reset map for Tailed SLIP "Stepping" (setting the leg touchdown angle $\theta_{\mathrm{td}+}$ as a function of the liftoff state, θ_{lo}, and a desired leg angular momentum $a_{\mathbf{h}}^*$) can be used to control forward speed for a pendular walking/running system [10]. In particular, a slight modification of the "scissor algorithm" [10, Chap. 5] yields

$$\theta_{\mathrm{td}} = -\theta_{\mathrm{lo}} + u_{\mathbf{h}}, \text{where } u_{\mathbf{h}} := k_{\mathbf{h}}(a_{\mathbf{h}}^* - a_{\mathbf{h}}), \tag{23}$$

Assumption 3 also simplifies the flight map, since the CoM flight behavior is well represented by a ballistic motion. The guard set for the "flight" reset is identical to that for the embedded radial coordinate r (Section 3.1), $G(a_{\mathbf{v}}, a_{\mathbf{h}}, t) = G_{\mathbf{v}}(a_{\mathbf{v}}, t)$

We transform the liftoff velocity vector into Cartesian coordinates, reflect the vertical component (ballistic flight) and transform back to polar coordinates to get

$$\begin{bmatrix} \rho\dot{\theta} \\ \dot{r} \end{bmatrix}_{\mathrm{td}+} = \mathrm{Rot}(-\theta_{\mathrm{td}+}) \begin{bmatrix} 1 & \\ & -1 \end{bmatrix} \mathrm{Rot}(\theta_{\mathrm{lo}}) \begin{bmatrix} \rho\dot{\theta} \\ \dot{r} \end{bmatrix}_{\mathrm{lo}},$$

and as a last step we can substitute in (23) with $a := \begin{bmatrix} a_{\mathbf{h}} \\ a_{\mathbf{v}} \end{bmatrix}$ (with the components as defined just before (19), (22)) to get

$$a_{\mathrm{td}+} = \begin{bmatrix} 1 & \\ & -1 \end{bmatrix} \begin{bmatrix} \rho & \\ & 1 \end{bmatrix} \mathrm{Rot}(-\theta_{\mathrm{td}+}) \begin{bmatrix} 1 & \\ & -1 \end{bmatrix} \mathrm{Rot}(\theta_{\mathrm{lo}}) \begin{bmatrix} 1/\rho & \\ & 1 \end{bmatrix} a_{\mathrm{lo}}$$

$$\implies \mathcal{R}(a) \stackrel{(23)}{=} \begin{bmatrix} \cos u_{\mathbf{h}} & -\rho \sin u_{\mathbf{h}} \\ \sin u_{\mathbf{h}}/\rho & \cos u_{\mathbf{h}} \end{bmatrix} a. \tag{24}$$

As apparent from (24), this map does not depend upon the leg angle, θ (from (23), $u_{\mathbf{h}}$ only depends on $\dot{\theta}$). Together with the equivariance of the continous dynamics with θ (assumption 2), this allows us to work in the $a_{\mathbf{h}}$-quotient space (as in Sec-

tion 3.2). A drawback of this reduction is that the hopping system exhibits pairs of antisymmetric steps [10, Chap. 5]: a period-2 evolution of non-neutral stances which are each mirror-symmetric to the subsequent step. In our empirical trials, with small leg sweep (assumption 4) we did not observe any significantly skewed stances.

Existence of periodic orbits With fixed $k_{\mathbf{v}}$ (and by (17), $a_{\mathbf{t}}$) the averaged fields (19), (21) yield simple flows of the form

$$\overline{f^\pi}(a) = \begin{bmatrix} a_{\mathbf{h}} - \nu_1, \\ \nu_2 a_{\mathbf{v}} + \nu_3 \end{bmatrix}, \tag{25}$$

where $a := (a_{\mathbf{h}}, a_{\mathbf{v}})$, ν_1, $0 < \nu_2 < 1$ and ν_3 are constants depending only on $k_{\mathbf{v}}$ and system parameters.

The zeros of $Q(a) = a - \mathcal{R} \circ \overline{f^\pi}(a)$ lie on periodic orbits of the averaged system. By the implicit function theorem, we only need to find an open neighborhood of a where $\mathrm{D}_a Q$ is full rank to check that periodic orbits exist. By design of $u_{\mathbf{h}}$, $k_{\mathbf{h}} \ll 1$ (before (13)), and so from (24),

$$\mathrm{D}_a \mathcal{R} = \begin{bmatrix} \cos u_{\mathbf{h}} & -\rho \sin u_{\mathbf{h}} \\ \sin u_{\mathbf{h}}/\rho & \cos u_{\mathbf{h}} \end{bmatrix} + \mathcal{O}(k_{\mathbf{h}}) \approx \begin{bmatrix} \cos u_{\mathbf{h}} & -\rho \sin u_{\mathbf{h}} \\ \sin u_{\mathbf{h}}/\rho & \cos u_{\mathbf{h}} \end{bmatrix}, \tag{26}$$

and so, combining with $\mathrm{D}\overline{f^\pi}$ from (25), $\mathrm{D}_a Q \approx I - \begin{bmatrix} 1 & \\ & \nu_2 \end{bmatrix} \begin{bmatrix} \cos u_{\mathbf{h}} & -\rho \sin u_{\mathbf{h}} \\ \sin u_{\mathbf{h}}/\rho & \cos u_{\mathbf{h}} \end{bmatrix}$, which is full rank as long as the right summand has no unity eigenvalues (sufficient condition). Since $\nu_2 < 1$, $u_{\mathbf{h}} \neq 0$ is sufficient to ensure this.

Proposition 3 (Stability). *Tailed SLIP limit cycles have locally stable return maps.*

Proof. We examine the stability properties of the discrete dynamical system $a \mapsto \overline{P}(a)$, the Jacobian of which factors into

$$\mathrm{D}_a \overline{P}|_a = \mathrm{D}_a(\overline{f^\pi} \circ \mathcal{R})|_a = \mathrm{D}_a \overline{f^\pi}|_{\mathcal{R}(a)} \cdot \mathrm{D}_a \mathcal{R}|_a. \tag{27}$$

Repeating the argument and calculation (26), for sufficiently small $k_{\mathbf{h}}$, $\mathrm{D}_a \overline{P}(a) = \begin{bmatrix} 1 & \\ & \nu_2 \end{bmatrix} \begin{bmatrix} \cos u_{\mathbf{h}} & -\rho \sin u_{\mathbf{h}} \\ \sin u_{\mathbf{h}}/\rho & \cos u_{\mathbf{h}} \end{bmatrix}$. The eigenvalues of $\mathrm{D}_a \overline{P}$ are in the stable region iff its determinant and trace satisfy (i) $\det < 1$, (ii) $\det > \mathrm{tr} - 1$, and (iii) $\det > -\mathrm{tr} - 1$. A simple calculation yields

$$\det(\mathrm{D}_a \overline{P}) = \nu_2, \quad \mathrm{tr}(\mathrm{D}_a \overline{P}) = (1 + \nu_2) \cos u_{\mathbf{h}}, \tag{28}$$

and since $0 < \nu_2 < 1$, $\mathrm{D}_a \overline{P}$ has stable eigenvalues. $\square$

5 Numerical and Empirical Results

The theoretical development in this paper is motivated by the implementation of tail-energized hopping on the Penn Jerboa [12], a tailed monopedal robot (with co-
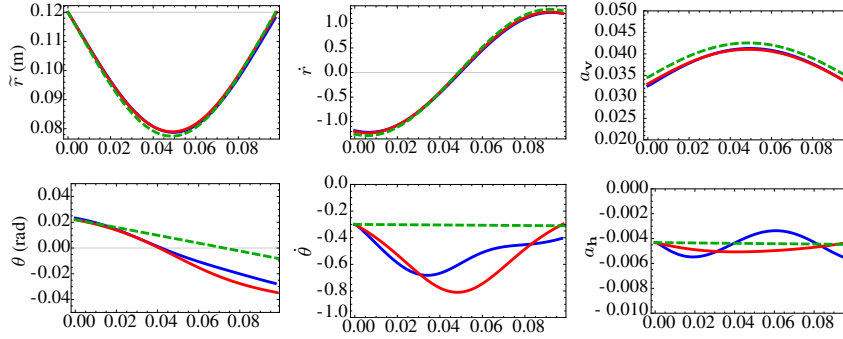
Fig. 4 Results from numerical simulation showing the evolution of various coordinates during a single stance phase: full Jerboa [12] simulation (no assumption 3, analytically intractable) with pitch immobilized (blue), tailed SLIP as modeled in this paper (15) (red), and the isolated templates of Section 3 (green).

incident hip and tail axes) in the sagittal plane. To demonstrate different facets of the ideas presented here, we present both simulation results, as well as experiments on the physical hardware.

Relationship to model (Section 4) The model presented earlier in the paper is a reasonable representation of the physical platform, but with the distinctions

- the robot has an additional "body pitch" DOF, which we immobilize using a boom for our experiments, and
- the tail actuator on the robot is attached between the tail and the body, whereas in the model it is attached between the tail and leg. For small leg sweep (assumption 4), the empirical behavior of either appears to be very similar.

Assumption 3 is reasonably satisfied by the physical platform: the tail mass is 0.15 kg, tail length is 0.3 m, while the body mass and inertia are (approx) 2.27 Kg and 0.025 Kg-m^2 respectively. That is, the tail mass is 6.6% of body mass, but tail inertia is 54% of body inertia. The overall control architecture of the robot is implemented as in Table 1.

Numerical simulation Fig. 4 shows simulation traces at (or near) a limit cycle for different plant models. The various parameters used in the simulation (matched to the robot hardware as much as possible): $m = 2.27$ Kg, $\rho = 0.12$ m, $m_t = 0.15$ Kg, $\rho_t = 0.3$ m, $\omega = 36.35$ rad/s, and $\varepsilon k_{\mathbf{v}} = 0.118$. The template plants and the analytically intractable Jerboa simulations both simulations all attracted to a steady-state hopping behavior, and we picked the "limit cycle" stance trajectories for Fig. 4 by simply allowing the simulation to run for some time.

The effect of averaging is apparent in the traces: while the qualitative system behavior is identical for the various plant models, the red and blue curves suffer from periodic, within-stance, perturbations (mechanical coupling interactions that we reimagine as time-varying disturbances to be "integrated out.").
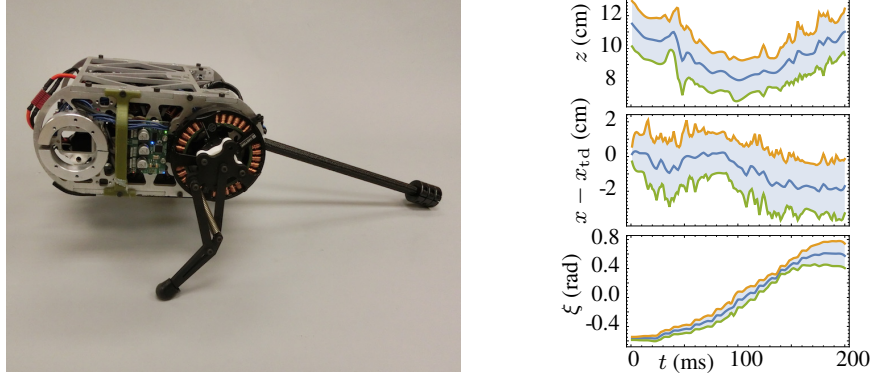
Fig. 5 Left: The physical platform used in this paper, the Penn Jerboa [12]. **Right:** stance data (mean and standard deviation) for a single trial on the robot, averaged over 36 steps. The z and x traces show rough profile comparable to the r, θ profiles in Fig. 4 modulo the polar transform (which leaves the profiles intact for small leg angles as we have assumed in assumption 4), and the ξ traces shows the expected profile (17) with our sinusoidal driving input.
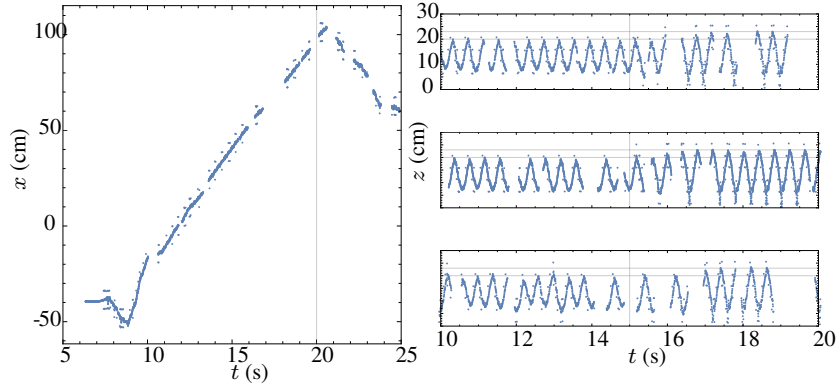
Fig. 6 We demonstrate stability and control authority over the hopping behavior by plotting (ground truth) fore-aft (**left**) and vertical (**right**) position for two trials where we imposed a step change in the desired energy levels, $a_{\mathbf{h}}$ (reversed at $t = 20$ s in the left plot) and $a_{\mathbf{v}}$ (increased by 33% at $t = 15$ s in the right plots). The "gaps" in the data are due to unfortunate communication dropouts with the instrumented boom.

Additionally, the gain scaling effect showed in Fig. 3 can be seen in the rightmost column of Fig. 4. For the same $k_{\mathbf{v}}$ and other parameters, the body (red, blue) has lower vertical energy and higher fore-aft energy than the template (green dashed).

Robot experiments For Jerboa [12] experiments, we constrain out-of-plane motion as well as body pitch using a boom. Qualitatively, the robot can hop stably (in multiple trials we recorded approximately 50 steps, and the experiment was terminated before failure), at limited speeds forward, backward, or in place. We have documented some trials in the supplementary video [22]. Fig. 6 shows ground-truth time series data from the instrumented boom demonstrating that the tail-energized

Table 2 Summary of 7 in-place hopping trials with height transition.

	Pre-transition		Post-transition	
Increase in $k_{\mathbf{v}}$	Mean ascent (cm)	Std. dev. (cm)	Mean ascent (cm)	Std. dev. (cm)
33 %	8.87692	3.14861	10.2622	4.34376

hopping strategy can attain stable hopping with tunable hopping height and fore-aft speed. Note that the high-frequency noise is caused by parasitic oscillations in the boom tube (which can be seen in the supplementary video [22]), and the blank portions are due to communication stalls in the data collection system.

In the left plot, the desired forward hopping speed is reversed at $t = 20\,\mathrm{s}$ and it can be seen that the robot begins hopping backwards in a few strides.

In the in-place hopping trials (right), $k_{\mathbf{v}}$ is increased 33% at $t = 15\,\mathrm{s}$, and we can see that within around three strides, the hopping height increases to a new equilibrium value. Table 2 shows some statistics on these trials (the gathered data from 7 of the 12 trials was usable, with large communication drops in the remaining). Qualitatively, the robot stably switched between two hopping heights in each run.

6 Conclusion

To sum up the contributions of this paper, we (a) motivate, propose, and demonstrate a new, relaxed, notion of anchoring using our extension (Section 2) of classical averaging theory, (b) show that in a decoupled implementation (Table 1) of tail-energized hopping in an idealized (assumptions 1-4) planar tailed monoped (15), the stance vector field decomposes in an averaged sense (but not in an exact sense) to a 1DOF vertical hopper and active rimless wheel (Prop. 2), and (c) give a proof of stability (Prop. 3) for the tailed monoped (d) test numerically and through experiments (Section 5) that the same feedback control rules stabilize planar hopping on the Jerboa [12] with controllable height and forward speed.

Future work We next plan to develop a formal definition of average anchoring (which we have skirted in this paper in favor of an illustration using the tailed monoped example), as well as an investigation into its relation to the classical anchoring notion [3].

The physical platform we have used, the Jerboa, has 12 unconstrained DOF's [12], but our tailed monoped model in this paper considers only 5 of them (2DOF body, 2DOF leg, 1DOF tail). In future work, we wish to explore the composition of more templates with the ones in Section 3 (as suggested in [11]), in order to be able to detach the robot from the boom.

References

1. J. Guckenheimer and P. Holmes, *Nonlinear Oscillations, Dynamical Systems, and Bifurcations of Vector Fields*. Applied Mathematical Sciences, Springer New York, 1990.
2. P. Holmes, R. J. Full, D. E. Koditschek, and J. Guckenheimer, "The dynamics of legged locomotion: Models, analyses, and challenges," *SIAM Review*, vol. 48, no. 2, pp. 207–304, 2006.
3. R. J. Full and D. E. Koditschek, "Templates and anchors: neuromechanical hypotheses of legged locomotion on land," *Journal of Exp. Biology*, vol. 202, pp. 3325–3332, Dec. 1999.
4. M. Buhler, D. E. Koditschek, and P. J. Kindlmann, "A family of robot control strategies for intermittent dynamical environments," *Control Systems Magazine, IEEE*, vol. 10, no. 2, pp. 16–22, 1990.
5. J. Nakanishi, T. Fukuda, and D. E. Koditschek, "A brachiating robot controller," *IEEE Transactions on Robotics and Automation*, vol. 16, no. 2, pp. 109–123, 2000.
6. U. Saranli, W. J. Schwind, and D. E. Koditschek, "Toward the control of a multi-jointed, monoped runner," in *1998 IEEE International Conference on Robotics and Automation*, vol. 3, pp. 2676–2682, 1998.
7. U. Saranli and D. E. Koditschek, "Template based control of hexapedal running," in *Robotics and Automation, 2003. Proceedings. ICRA'03. IEEE International Conference on*, vol. 1, pp. 1374–1379, IEEE, 2003.
8. J. W. Grizzle, C. Chevallereau, R. W. Sinnet, and A. D. Ames, "Models, feedback control, and open problems of 3d bipedal robotic walking," *Automatica*, vol. 50, pp. 1955–1988, Aug. 2014.
9. E. Westervelt and J. Grizzle, *Feedback Control of Dynamic Bipedal Robot Locomotion*. Control and Automation Series, CRC PressINC, 2007.
10. M. Raibert, *Legged Robots that Balance*. Artificial Intelligence, MIT Press, 1986.
11. A. De and D. E. Koditschek, "Parallel composition of templates for tail-energized planar hopping," in *Robotics and Automation (ICRA), 2015 IEEE International Conference on*, pp. 4562–4569, May 2015.
12. A. De and D. E. Koditschek, "The Penn Jerboa: A platform for exploring parallel composition of templates," tech. rep., University of Pennsylvania, Feb 2015. arXiv:1502.05347.
13. D. E. Koditschek and M. Buehler, "Analysis of a simplified hopping robot," *The International Journal of Robotics Research*, vol. 10, pp. 587–605, Dec. 1991.
14. J. Bhounsule, J. Cortell, and A. Ruina, "Design and control of ranger: an energy-efficient, dynamic walking robot," in *Proc. CLAWAR*, pp. 441–448, 2012.
15. H. Khalil, *Nonlinear Systems*. Prentice Hall, 3rd ed., 2002.
16. T. McGeer, "Passive dynamic walking," *International Journal of Robotics Research*, vol. 9, no. 2, pp. 62–82, 1990.
17. G. Secer and U. Saranli, "Control of monopedal running through tunable damping," in *2013 21st Signal Processing and Communications Applications Conference (SIU)*, pp. 1–4, Apr. 2013.
18. R. Blickhan and R. Full, "Similarity in multilegged locomotion: bouncing like a monopode," *Journal of Comparative Physiology A*, vol. 173, no. 5, pp. 509–517, 1993.
19. S. Burden, S. Revzen, and S. S. Sastry, "Dimension reduction near periodic orbits of hybrid systems," in *2011 50th IEEE Conference on Decision and Control and European Control Conference (CDC-ECC)*, pp. 6116–6121, IEEE, 2011.
20. H. Geyer, A. Seyfarth, and R. Blickhan, "Spring-mass running: simple approximate solution and application to gait stability," *Journal of theoretical biology*, vol. 232, no. 3, pp. 315–328, 2005.
21. E. W. Weisstein, "Bessel Function of the First Kind," 2015. From MathWorld–A Wolfram Web Resource. http://mathworld.wolfram.com/BesselFunctionoftheFirstKind.html.
22. A. De, "Supplementary material for this paper," 2015. http://kodlab.seas.upenn.edu/Avik/AveragingTSLIP.